IMPACT OF DOUBLE-DIFFUSION AND SECOND ORDER SLIP ON CONVECTION OF CHEMICALLY REACTING OLDROYD-B LIQUID WITH CATTANEO-CHRISTOV DUAL FLUX

by

Fouad Othman M. MALLAWI [a], ***Sheniyappan ESWARAMOORTHI*** [b], ***Marimuthu BHUVANESWARI*** [c], ***and Sivanandam SIVASANKARAN*** [a*]

[a] Department of Mathematics, King Abdulaziz University, Jeddah, Saudi Arabia
[b] Department of Mathematics, Dr. N.G.P. Arts and Science College, Coimbatore, Tamilnadu, India
[c] Department of Mathematics, Kongunadu Polytechnic College, D.Gudalur, Dindigul, Tamilnadu, India

Original scientific paper
https://doi.org/10.2298/TSCI191003214M

This article express the outcomes of mixed convective flow of a chemically reacting Oldroyd-B liquid with Cattaneo-Christov double flux under the consequence of second order slip, heat absorption/heat generation and Newtonian cooling/Newtonian heating. The governing PDE are converted into ODE using suitable variables. The homotopy analysis method is employed to solve these resultant equations. The outcomes of diverse physical parameters, like, relaxation time, retardation time, Richardson number, buoyancy ratio, Prandtl number, radiation, heat absorption/generation, Schmidt number, chemical reaction, suction/injection, slip and Newtonian heating are discussed.

Key words: *Oldroyd-B liquid, Cattaneo-Christov double flux, Newtonian heating, homotopy analysis method, heat generation, second order slip*

Introduction

The non-Newtonian liquids play a vital role in industry, engineering, pharmaceuticals, *etc*. Example of such liquids are shampoos, sugar solutions, polymeric liquids, blood, inks and it cannot illustrated as a linear constitutive model. Many liquid models were developed to exhibit the features of non-Newtonian liquids. Usually non-Newtonian liquids can be segregated as liquids of rate, differential and integral types. Among these classification, rate type liquids were considered for memory and elastic effects. One of the simplest rate type of liquid is Oldroyd-B liquid (OBL) and this liquid predicts the retardation and relaxation time characteristics. This liquid was initiated by Oldroyd [1] in 1950. It is useful in chemical and process industry when they encounter both the elastic and memory effects exhibited by most biological and polymers liquids. Rajagopal and Bhatnagar [2] derived the exact solution of simple OBL. Analytical solution of 3-D OBL with Soret and Dufour effects were derived by Farooq *et al*. [3]. Several studies about OBL flow are found in under different conditions are Fetecau *et al*. [4], Liu *et al.* [5], Jamil *et al*. [6], and Motsa and Ansari [7].

Heat transfer mechanism is a natural phenomenon and it occurs due to variations of temperature within the same object or between bodies and this is very useful in many industrial processes, like, cooling of nuclear reactor, power generation, electronic devices cooling and

* Corresponding author, e-mail: sd.siva@yahoo.com

magnetic drugs targeting. Fourier [8] initiated *Fouriers law of heat conduction* and there is no material satisfy this law. Then, Cattaneo [9] made some modification by including a relaxation time parameter for heat flux in order to avoid the paradox of heat conduction. After that, Christov [10] improved the Cattaneo model by introducing the thermal relaxation time with Oldroyds upper-convected derivatives to reach the material invariant formulation. The outcome of upper-convected Maxwell fluid with Cattaneo-Christov (CC) model with heat generation was investigated by Asmadi *et al.* [11]. They noticed that the lower amount of heat transfer gradient gets in the presence of thermal relaxation time parameter. The CC heat flux model was successfully used in OBL by Mustafa [12], in Maxwell nanofluid by Sui *et al*. [13], in nanofluid by Dogonchi and Ganji [14], in second grade fluid by Mallawi *et al*. [15], and in Maxwell fluid by Khan *et al*. [16].

The transfer of energy from the surface is proportional to the temperature local surface is treated as Newtonian heating (NH). The NH has significant applications in engine cooling, thermal energy storage, nuclear turbines, heat exchanger, petroleum industry, solar radiation, *etc*. The NH of a MHD OBL flow was investigated by Mehmood *et al*. [17]. They found that the energy enhances with enhancing the NH parameter. Few significant important studies in this area are found in [18-20]. No-slip boundary conditions are not sufficient in micro-electro mechanical systems. Because there is no relative motion between the surface and liquid immediately in contact with the surface. But slip flow model exhibits the relation between the velocity of the surface and velocity gradient normal to the surface. The flow of chemically reactive nanofluid with radiation and second order slip was portrayed by Zhu *et al*. [21]. They found the fluid temperature rises with the presence of second order velocity slip and the reverse trend was obtained with first order velocity slip case. Velocity slip of a Oldroyd-B nanoliquid-flow over a permeable stretching sheet with heat generation (HG) absorption was examined by Das *et al*. [22]. They showed that the heat transfer gradient declines when raising the velocity slip parameter. Slip flow of a MHD Jeffrey nanofluid-flow with radiation and triple stratification was pedantically solved by Jagan *et al*. [23]. They proved that the fluid velocity reduces when rising the velocity slip parameter.

From the aforementioned literature studies indicate that, chemically reacting fluid-flow of an OBL with Cattaneo-Christov double flux (CCDF) flux and second order velocity slip has not studied yet. This analysis carried out the impact of second order velocity slip and Newtonian heating on OBL over a stretchy plate with HG/heat absorption (HA), chemical reaction and CCDF.

Mathematical formulation

We consider the 2-D flow of an OBL towards a stretchy plate. Let $\hat{U}_w = A\hat{x}$ be the plate velocity, $A > 0$ is the constant. The surface of the plate is adopted with partial slip condition. The plate is kept at unvarying temperature $\hat{T}_w$ and concentration $\hat{C}_w$ which is higher than the free stream temperature $\hat{T}_\infty$ and concentration $\hat{C}_\infty$. The heat transfer phenomenon is calculated in the presence of Newtonian cooling (NC)/NH. It is assumed that the liquid is a gray, absorbing and emitting. The Rosseland diffusion model is employed for thermal radiation. Thermal and solutal buoyancy effects are taken into account. Time independent destructive and constructive chemical reactions are considered here, [24-27]. The CCDF model was incorporated for analyzing the variations of mass and hear transfer. In addition, the energy equation is modeled with HA/HG. The governing boundary-layer equations under CCDF are given:

$$\frac{\partial \hat{u}_1}{\partial \hat{x}} + \frac{\partial \hat{u}_2}{\partial \hat{y}} = 0 \tag{1}$$

$$\hat{u}_1\frac{\partial\hat{u}_1}{\partial\hat{x}}+\hat{u}_2\frac{\partial\hat{u}_1}{\partial\hat{y}}+\hat{\lambda}_1\left(\hat{u}_1^2\frac{\partial^2\hat{u}_1}{\partial\hat{x}^2}+\hat{u}_1^2\frac{\partial^2\hat{u}_1}{\partial\hat{y}^2}+2\hat{u}_1\hat{u}_2\frac{\partial^2\hat{u}_1}{\partial\hat{x}\partial\hat{y}}\right)=$$
$$=\hat{g}\left(\beta_{\hat{T}}\left[\hat{T}-\hat{T}_\infty\right]+\beta_{\hat{C}}\left[\hat{C}-\hat{C}_\infty\right]\right)$$
$$+\nu\left(\frac{\partial^2\hat{u}_1}{\partial\hat{y}^2}+\hat{\lambda}_2\left[\hat{u}_1\frac{\partial^3\hat{u}_1}{\partial\hat{y}^2\partial\hat{x}}+\hat{u}_2\frac{\partial^3\hat{u}_1}{\partial\hat{y}^3}-\frac{\partial^2\hat{u}_1}{\partial\hat{y}^2}\frac{\partial\hat{u}_1}{\partial\hat{x}}-\frac{\partial^2\hat{u}_2}{\partial\hat{y}^2}\frac{\partial\hat{u}_1}{\partial\hat{y}}\right]\right) \tag{2}$$

$$\hat{u}_1\frac{\partial\hat{T}}{\partial\hat{x}}+\hat{u}_1\frac{\partial\hat{T}}{\partial\hat{y}}+\hat{\lambda}^3\hat{\Omega}_{\hat{T}}=\hat{\alpha}\frac{\partial^2\hat{T}}{\partial\hat{y}^2}+\hat{\alpha}\frac{16\sigma^*\hat{T}_\infty^3}{3kk^*}\frac{\partial^2\hat{T}}{\partial\hat{y}^2}+\frac{Q}{\rho C_p}\left(\hat{T}-\hat{T}_\infty\right) \tag{3}$$

$$\hat{u}_1\frac{\partial\hat{C}}{\partial\hat{x}}+\hat{u}_2\frac{\partial\hat{C}}{\partial\hat{y}}+\hat{\lambda}^4\hat{\Omega}_{\hat{C}}=\hat{D}_B\frac{\partial^2\hat{C}}{\partial\hat{y}^2}-k_1\left[\hat{C}-\hat{C}_\infty\right] \tag{4}$$

where $(\hat{u}_1, \hat{u}_2)$ are the velocity components in $(\hat{x}, \hat{y})$ co-ordinates, ν – the kinematic viscosity, $(\hat{\lambda}_1, \hat{\lambda}_2)$ – the relaxation and retardation time parameters, $\hat{g}$ – the acceleration due to gravity, $(\beta_{\hat{T}}, \beta_{\hat{C}})$ – the coefficients of thermal and concentration expansions, $(\hat{\lambda}_3, \hat{\lambda}_4)$ – the relaxation time of heat and mass fluxes, $\hat{\alpha}$ – the thermal diffusivity, ρ – the density, C_p – the specific heat capacity, σ – the Stefan Boltzmann constant, k – the thermal conductivity, k^* – the mean absorption coefficient, Q – the heat absorption/generation coefficient, $\hat{D}_B$ – the mass diffusivity, and k_1 – the chemical reaction rate.

The relaxation time of heat and mass fluxes are:

$$\Omega_{\hat{T}}=\hat{u}_1\frac{\partial\hat{u}_1}{\partial\hat{x}}\frac{\partial\hat{T}}{\partial\hat{x}}+\hat{u}_2\frac{\partial\hat{u}_2}{\partial\hat{y}}\frac{\partial\hat{T}}{\partial\hat{y}}+\hat{u}_1^2\frac{\partial^2\hat{T}}{\partial\hat{x}^2}+\hat{u}_2^2\frac{\partial^2\hat{T}}{\partial\hat{y}^2}+2\hat{u}_1\hat{u}_2\frac{\partial^2\hat{T}}{\partial\hat{x}\partial\hat{y}}+\hat{u}_1\frac{\partial\hat{u}_2}{\partial\hat{x}}\frac{\partial\hat{T}}{\partial\hat{y}}+\hat{u}_2\frac{\partial\hat{u}_1}{\partial\hat{y}}\frac{\partial\hat{T}}{\partial\hat{x}}$$

$$\Omega_{\hat{C}}=\hat{u}_1\frac{\partial\hat{u}_1}{\partial\hat{x}}\frac{\partial\hat{C}}{\partial\hat{x}}+\hat{u}_2\frac{\partial\hat{u}_2}{\partial\hat{y}}\frac{\partial\hat{C}}{\partial\hat{y}}+\hat{u}_1^2\frac{\partial^2\hat{C}}{\partial\hat{x}^2}+\hat{u}_2^2\frac{\partial^2\hat{C}}{\partial\hat{y}^2}+2\hat{u}_1\hat{u}_2\frac{\partial^2\hat{C}}{\partial\hat{x}\partial\hat{y}}+\hat{u}_1\frac{\partial\hat{u}_2}{\partial\hat{x}}\frac{\partial\hat{C}}{\partial\hat{y}}+\hat{u}_2\frac{\partial\hat{u}_1}{\partial\hat{y}}\frac{\partial\hat{C}}{\partial\hat{x}}$$

with the boundary conditions:

$$\hat{u}_1=A\hat{x}+\hat{L}_1\frac{\partial\hat{u}_1}{\partial\hat{y}}+\hat{L}_2\frac{\partial^2\hat{u}_1}{\partial\hat{y}^2},\ \hat{u}_2=V_w(x),\ \frac{\partial\hat{T}}{\partial\hat{y}}=-\hat{h}_c\hat{T},\ \hat{C}=\hat{C}_w\ \text{ at }\ \hat{y}=0$$
$$\widehat{u_1}\to 0,\ \frac{\partial\widehat{u_1}}{\partial\hat{y}}\to 0,\ \hat{T}\to\hat{T}_\infty,\ \hat{C}\to\hat{C}_\infty\ \text{ at }\ \hat{y}\to\infty \tag{5}$$

Now, the following dimensionless variables are introduced:

$$\eta=\hat{y}\sqrt{\frac{A}{\nu}},\ \ \hat{u}_1=\overline{x}AF',\ \ \hat{u}_2=-\sqrt{\nu A}F,\ \ \Theta=\frac{\hat{T}-\hat{T}_\infty}{\hat{T}_\infty},\ \ \Phi=\frac{\hat{C}-\hat{C}_\infty}{\hat{C}_w-\hat{C}_\infty} \tag{6}$$

$$F'''-F'^2+F''F+\alpha_1\left[2F''F'F-F'''F^2\right]+\alpha_2\left[F''^2-F^{iv}F\right]+\mathrm{Ri}\left[\Theta+N\Phi\right]=0 \tag{7}$$

$$\frac{1}{\mathrm{Pr}}\left[\frac{4}{3}R+1\right]\Theta''+\Theta'F-\Gamma_T\left[\Theta'F'F+\Theta''F^2\right]+Hg\Theta=0 \tag{8}$$

$$\frac{1}{\mathrm{Sc}}\Phi''+\Phi'F-\Gamma_C\left[\Phi'F'F+\Phi''F^2\right]-Cr\Phi=0 \tag{9}$$

with the conditions

$$F(0)=F_w,\ F'(0)=1+\Delta_1 F''(0)+\Delta_2 F'''(0)$$
$$\Theta'(0)=-N_T\left[1+\Theta(0)\right],\ \Phi(0)=1,\ F'(\infty)=0,\ \Theta(\infty)=0,\ \Phi(\infty)=0 \tag{10}$$

where $\alpha_1=\hat{\lambda}_1 A$ is the relaxation time constant, $\alpha_2=\hat{\lambda}_2 A$ – the retardation time constant, $\mathrm{Ri}=\mathrm{Gr}_x/\mathrm{Re}_x^2$ – the Richardson number, $\mathrm{Gr}_x=[g\beta_{\hat{T}}(\hat{T}_w-\hat{T}_\infty)\hat{x}^3]/\nu^2$ – the thermal buoyancy parameter, $\mathrm{Re}_x=A\hat{x}^2/\nu$ – the Reynolds number, $N=\mathrm{Gr}_x^*/\mathrm{Gr}_x=[g\beta_{\hat{C}}(\hat{C}_w-\hat{C}_\infty)]/[g\beta_{\hat{T}}(\hat{T}_w-\hat{T}_\infty)]$ – the ratio of concentration thermal buoyancy, $\mathrm{Gr}_x^*=[g\beta_{\hat{C}}(\hat{C}_w-\hat{C}_\infty)\hat{x}^3]/\nu^2]$ – the concentration buoyancy parameter, $\mathrm{Pr}=\nu/\hat{\alpha}$ – the Prandtl number, $R=(4\sigma^*\hat{T}_\infty^3)/kk^*$ – the thermal radiation parameter, $\Gamma_{\hat{T}}=\hat{\lambda}_3 A$ – the non-dimensional thermal relaxation time parameter, $Hg=Q/\rho C_p A$ – the heat generation/absorption parameter, $\mathrm{Sc}=\nu/\hat{D}_B$ – the Schmidt number, $\Gamma_{\hat{C}}=\hat{\lambda}_4 A$ – the non-dimensional solutal relaxation time parameter, $Cr=k_1/A$ – the chemical reaction parameter, $\Delta_1=L_1(A/\nu)^{1/2}$ – the first order slip parameter, $\Delta_2=L_2(A/\nu)^{1/2}$ – the second order slip parameter, and $N_T=\hat{h}_c(\nu/A)^{1/2}$ – the conjugate parameter.

The non-dimensional form of the skin friction coefficient, local Nusselt and Sherwood numbers:

$$\frac{1}{2}C_f\sqrt{\mathrm{Re}_x}=\frac{1+\alpha_1}{1+\alpha_2}F''(0),\quad \frac{\mathrm{Nu}}{\sqrt{\mathrm{Re}_x}}=B_T\left(1+\frac{4}{3}R\right)\left(1+\frac{1}{\theta(0)}\right),\quad \text{and}\quad \frac{\mathrm{Sh}}{\sqrt{\mathrm{Re}_x}}=-\Phi'(0)$$

The homotopy analysis method solutions

The obtained eqs. (7)-(9) with boundary conditions (10) are solved using homotopy analysis method (HAM). We assume the initial approximations:

$$F_0(\eta)=F_w+\eta\exp(-\eta)+\frac{3\Delta_2-2\Delta_1}{\Delta_2-1-\Delta_1}\exp(-\eta)-\frac{3\Delta_2-2\Delta_1}{\Delta_2-1-\Delta_1}$$

$$\Theta_0(\eta)=\frac{N_T}{1-N_T}\exp(-\eta)\ \text{and}\ \Phi_0(\eta)=\exp(-\eta)$$

The linear operators are:

$$L_F=\frac{\mathrm{d}^3F}{\mathrm{d}\eta^3}-\frac{\mathrm{d}F}{\mathrm{d}\eta},\ L_\Theta=\frac{\mathrm{d}^2\Theta}{\mathrm{d}\eta^2}-\Theta\ \text{and}\ L_\Phi=\frac{\mathrm{d}^2\Phi}{\mathrm{d}\eta^2}-\Phi$$

with the conditions

$$L_F\left[E_1+E_2\exp(\eta)+E_3\exp(-\eta)\right]=0$$
$$L_\Theta\left[E_4\exp(\eta)+E_5\exp(-\eta)\right]=0,\ L_\Phi\left[E_6\exp(\eta)+E_7\exp(-\eta)\right]=0$$

where E_k ($k=1$-7) are arbitrary constants. After substituting the M^{th} order HAM equations, we get

$$F_M(\eta)=F_M^o(\eta)+C_1+C_2\exp(\eta)+C_3\exp(-\eta)$$
$$\Theta_M(\eta)=\Theta_M^o(\eta)+C_4\exp(\eta)+C_5\exp(-\eta)$$
$$\Phi_M(\eta)=\Phi_M^o(\eta)+C_6\exp(\eta)+C_7\exp(-\eta)$$

where $F_M^o(\eta)$, $\Theta_M^o(\eta)$, and $\Phi_M^o(\eta)$ are the particular solutions. In general, the HAM solutions have auxiliary parameter, namely h_F, h_Θ, and h_Φ which control the solution convergence, Bhuvaneswari *et al.* [28]. Figure 1 shows the range values of h_F, h_Θ, and h_Φ and the ranges are $-1.6\le h_F\le -0.3$, $-2\le h_\Theta\le 0.0$, $-1.7\le h_\Phi\le -0.2$. We choose $h_F=h_\Theta=h_\Phi=-1$ for the present calcula-

Table 1. Comparison of $-f''(0)$ for distinct values of α_1 with $\alpha_1 = 0$

α_1	[29]	[30]	Present study
0.0	0.99998	1.00000	1.00000
0.4	1.10185	1.10190	1.10190
0.8	1.19669	1.19671	1.19671
1.2	1.28525	1.28536	1.28536
1.6	1.36864	1.36876	1.3683

tion with 15[th] order of approximations. Table 1 shows the numerical value of $-f''(0)$ for distinct values of α_1 with $\alpha_2 = 0$ compared with Abel *et al.* [29] and Wagas *et al.* [30] and we proved that our results are in excellent agreement.

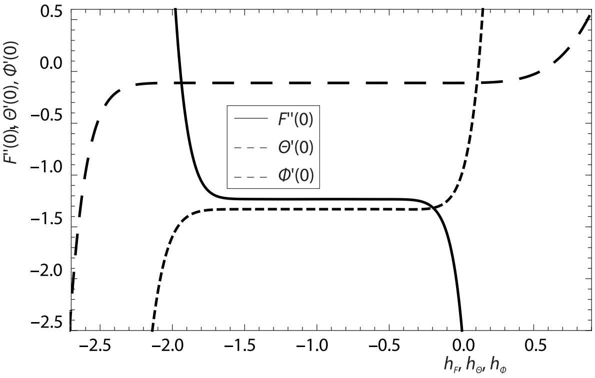

Figure 1. The *h* curves of $F''(0)$, $\Theta'(0)$, and $\Phi'(0)$ with $\alpha_1 = 0.1$, $\alpha_2 = 0.1$, Ri = 0.5, $N = 0.2$, Pr = 1.5, $R = 0.3$, $\Gamma_T = 0.1$, $Hg = -0.3$, Sc = 1.0, $\Gamma_C = 0.2$, $Cr = 1.0$, $F_w = 0.2$, $\beta_1 = 0.1$, $\beta_2 = 0.2$ and $N_T = 0.1$

Results and discussion

The outcomes of physical parameters, like, α_1, α_2, R, Γ_T, Hg, Γ_C, Cr F_w, Δ_1, Δ_2, and N_T, for fixed values of Richardson number (Ri = 0.5), buoyancy ratio parameter ($N = 0.2$), Prandtl number (Pr = 1.5), and Schmidt number (Sc = 1.0) are described in this section. Figures 2(a) and 2(b) give the impact of α_1 and α_2 for velocity profile. It is found that the stream speed becomes smaller when increasing the values of α_1. Physically, larger values of α_1 reveals to higher relaxation time component which against the liquid speed. This causes to suppress the liquid speed and thinner the associated boundary-layer thickness. On the contrary, the higher values of α_2 lead to enhance the liquid speed. The variations of R on heat absorbing and generating liquid with NH and cooling cases are illustrated in figs. 3(a) and 3(b). It is seen that the temperature grows for NH case and it diminishes for NC case. Physically, bigger thermal conjugate parameter is strengthening the heat transfer coefficient, which transfer more amount of energy from hotter place to cooler place. This means that increase the liquid temperature and thicken thermal boundary-layer thickness. On the contrary, negative values of N_T reduce the heat transfer coefficient and there by decreasing the liquid temperature. In addition, the thermal boundary-layer thickness is higher in heat generating liquid compared to the heat absorbing liquid. Because, the positive values of Hg (heat generation) is to increase the liquid thermal state and transfer more heat between liquid particles. This implies to enrich the thickness of thermal boundary-layer.

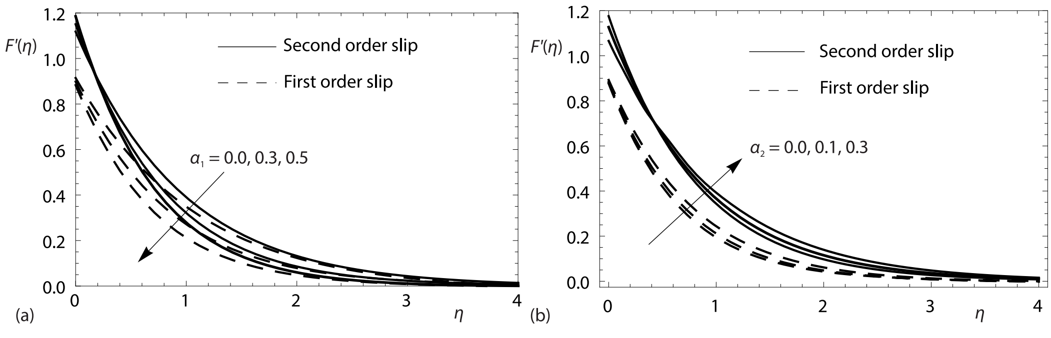

Figure 2. Impact of α_1 (a) and α_2 (b) on velocity profile

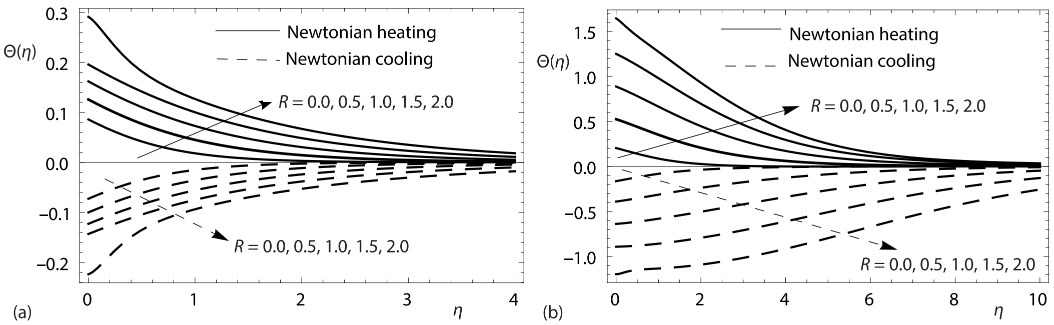

Figure 3. Impact of *R* on temperature profile for *Hg* = –0.3 (a) and *Hg* = 0.3 (b)

On the other hand, the negative values of *Ha* (heat absorption) is to create the opposite behavior and causes to reduction of thermal boundary-layer thickness.

Figures 4(a) and 4(b) portray the impact of Γ_T on temperature profile with and without thermal radiation for NH and cooling cases. It is observed that the liquid temperature and its corresponding boundary-layer thickness are suppressed by enhancing the thermal relaxation time parameter in NH case. The quite opposite behavior is obtained in NC case. In addition, the thermal boundary-layer thickness is high in the presence of radiation compared to the absence of radiation. Physically, higher amount of thermal radiation leads to increase the energy transport between particles and thereby increasing the thermal boundary-layer thickness. The effects of *Hg* on temperature profile for NH and cooling cases in the presence/absence of radiation are illustrated in figs. 5(a) and 5(b). It is found that the liquid temperature is an enhancing function of HG/HA parameter in NH case and the opposite trend is obtained in NC case. Also, the thicker boundary-layer gets at $R = 0.3$.

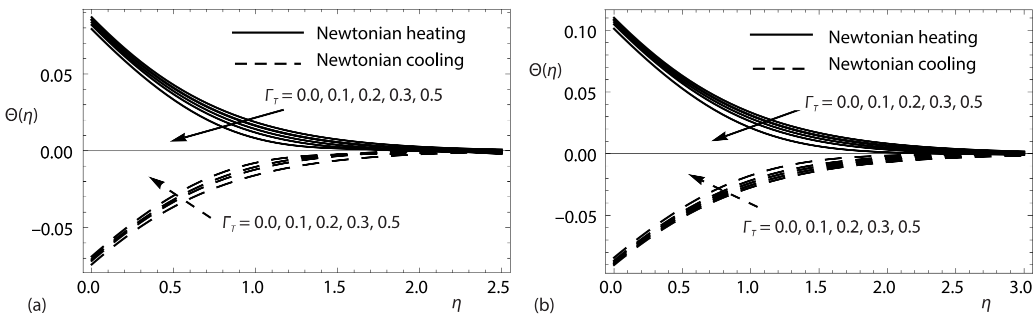

Figure 4. Impact of Γ_T on temperature profile for *R* = 0 (a) and *R* = 0.3 (b)

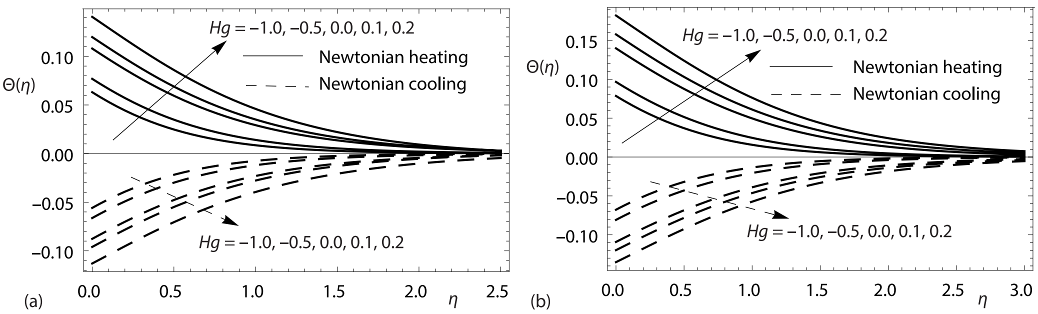

Figure 5. Impact of *Hg* on temperature profile for *R* = 0 (a) and *R* = 0.3 (b)

Figures 6(a) and 6(b) explain the variations of Γ_C in concentration profile for different types of chemical reactions and boundary conditions. It is seen that the liquid concentration and its associated boundary-layer thickness are suppressed when raising the concentration relaxation time for both boundary conditions. In generative chemical reaction, the liquid concentration overshoots near the surface and it starts to decay and finally tends to minimum (zero) value at $\eta \rightarrow \infty$. The effects of Cr on concentration profile for different boundary conditions with Fourier and non-Fourier mass fluxes are presented in figs. 7(a) and 7 (b). It is seen that the solutal boundary-layer thickness gets decay for enhancing the chemical reaction parameter. Also, we observed that boundary-layer gets thicken for non-Fourier case than the Fourier case. In addition, the decreasing rate is high in generative chemical reaction case compared to the destructive chemical reaction case.

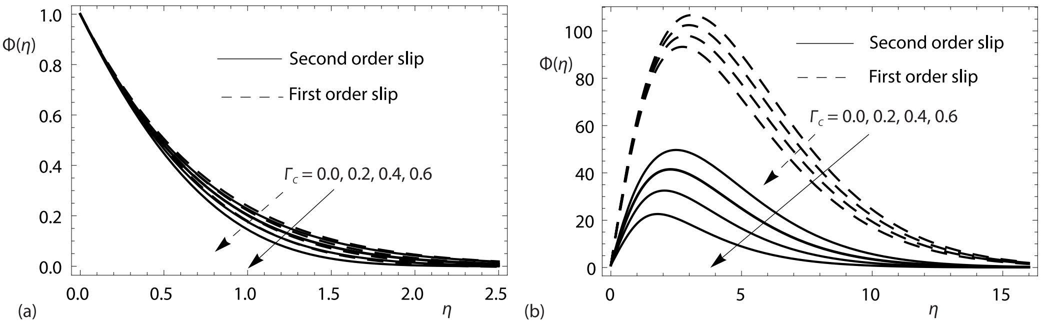

Figure 6. Impact of Γ_C on concentration profile for Cr = 1 (a) and Cr = –1 (b)

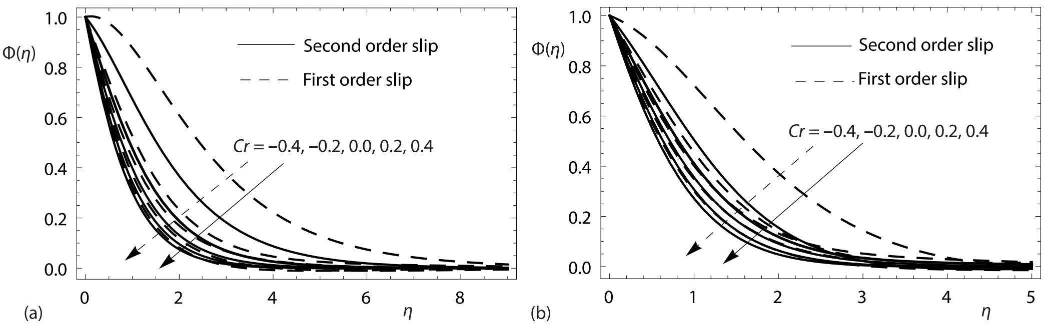

Figure 7. Impact of Cr on concentration profile for Γ_C = 0.0 (a) and Γ_C = 0.2 (b)

Figures 8(a) and (b) exhibit the comparative view of local Nusselt number for various values of Γ_T and Hg with NH, cooling, second order slip and first order slip parameters. It is found that the heat transfer gradient rises with raising the values of Γ_T and opposite behavior can be found for large values of Hg. The local Nusselt number is an enhancing function of thermal radiation parameter and the reverse trend is witnessed for higher values of Hg, figs. 9(a) and 9(b). In addition, the higher depression rate of heat transfer gradient is found when the larger heat transfer gradient is obtained in NH case compared to the cooling case. The similar trend is obtained for both second order slip and first order slip. The impact of Γ_C and Cr with heat generating, absorbing, second order slip and first order slip parameter is shown in figs. 10(a) and 10(b). We proved from this figures that, the mass transfer gradient enhances for larger values of Γ_C and Cr for all cases. The increasing rate of mass transfer is high in Fourier case compared to the non-Fourier case. It also observed that the mass transfer rate gets maximum in generative chemical reaction case.

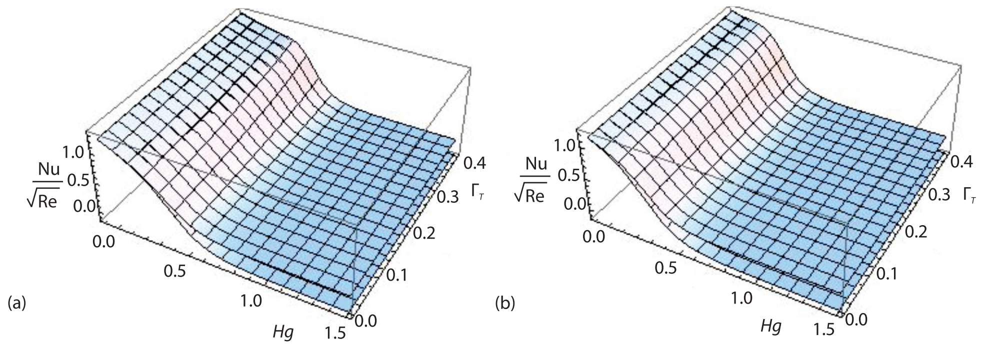

Figure 8. Variations Nu/(Re)$^{1/2}$ of for different values of *Hg* and Γ_T for second order slip; (a) and first order slip (b) with NH (upper profile) and NC (lower profile)

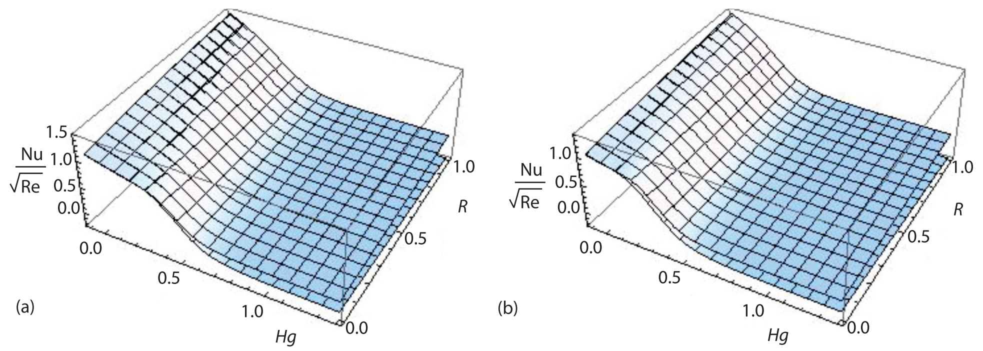

Figure 9. Variations of Nu/(Re)$^{1/2}$ for different values of *Hg* and *R* for second order slip (a) and first order slip (b) with NH (upper profile) and NC (lower profile)

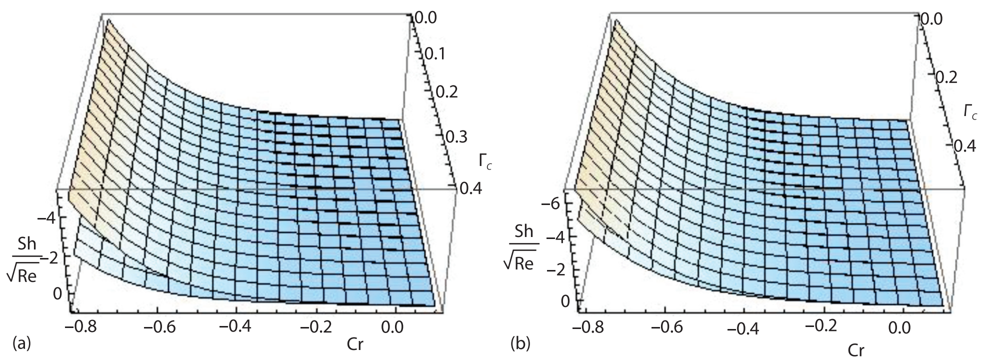

Figure 10. Variations of Sh/(Re)$^{1/2}$ for different values of *Cr* and Γ_C for heat generating (a) and heat absorption (b) with second order slip (lower profile) and first order slip (upper profile)

The increment/decrement of skin friction coefficient for distinct values of Hg, Δ_1, Δ_2, N_T is provided in figs. 11(a)-11(b). It is noted that the rate of skin friction coefficient decreases with respect to Hg, Δ_1, and Δ_2 for NH case, fig. 11(a). Higher amount of decreasing rate (189%) is observed for heat generating liquid with first order slip condition and NH case when $F_w = -0.2$. In NC case, we gained opposite trend, *i.e.*, higher amount of increment (2%) is attained at $F_w = -0.2$. Skin friction coefficient vanishes at $F_w = 0.0$ for heat generating liquid with first order

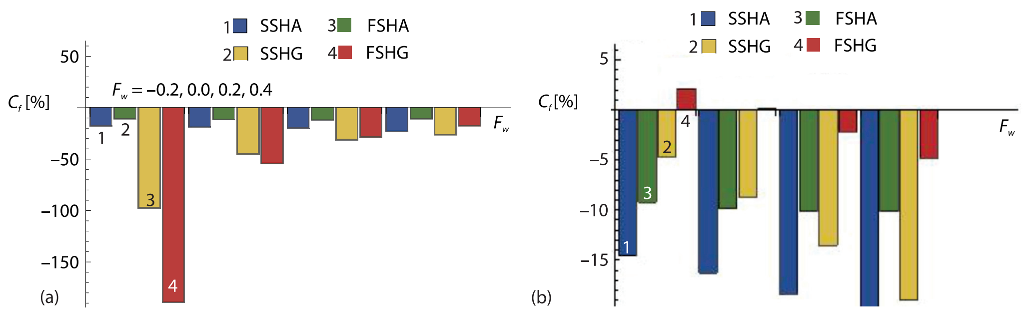

Figure 11. Variation percentage of skin friction coefficient for various values of F_w with HA/HG for NH (a) and NC (b)

slip and NC. Figures 12(a)-12(d) demonstrate the consequence of local Nusselt number with respect to Γ_T and R with SSHG, FSHG, SSHA, and FSHA for NH and NC cases. It is noticed that rate of change of local Nusselt number enhances when the values of Γ_T is rising, figs. 12(a) and 12(b). Also found that the higher amount of increment (17.4%) is obtained in NC case with SSHG at $\Gamma_T = 0.4$. From figs. 12(c) and 12(d), the local Nusselt number gets enhancement for HA case and it decays in the HG case. In addition, the decreasing percentage is close to zero when $R \to 1$. At $R = 0.3$, we obtained lager decrement (21.7%) in NC. The variation of local Sherwood number for different values of Γ_C and Cr with SSHG, FSHG, SSHA, and FSHA for NH and NC cases is provided in figs. 13(a) and 13(d). It is seen that the mass transfer gradient is an escalating function of Γ_C and Cr for all cases. From these figures, higher amount of mass transfer rate is observed in the presence of destructive chemical reaction. It is also observed that mass transfer rate declines when increasing the chemical reaction parameter for all the cases considered. The second order slip provides higher mass transfer rate for all vales of Γ_C and both cases of NH and NC.

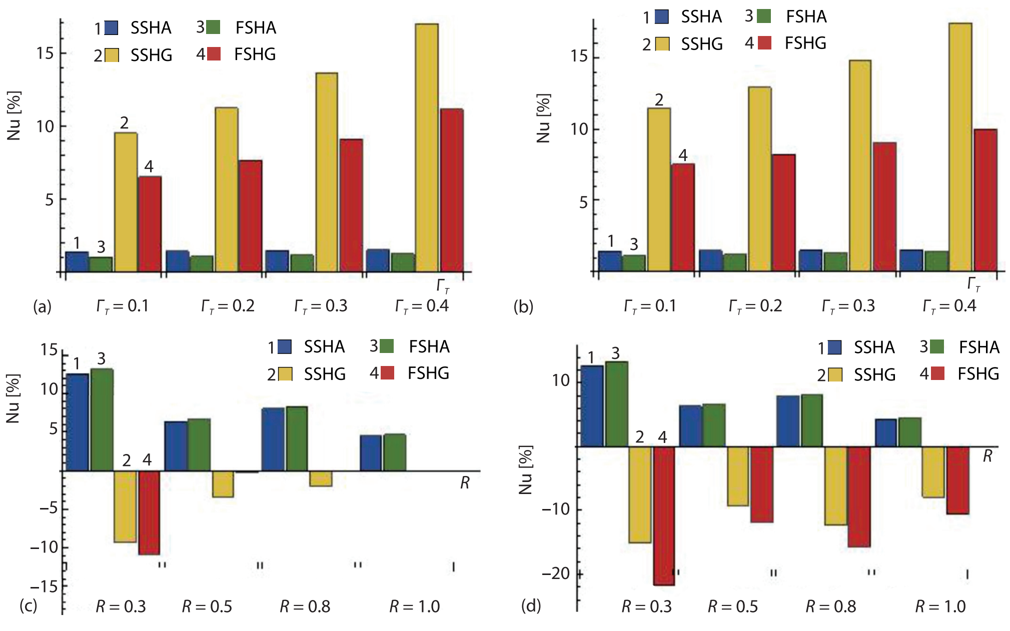

Figure 12. Variation percentage of local Nusselt number for various values of Γ_T (a) and (b) and R (c) and (d) with HA/HG for NH (a) and (c) and NC (b) and (d)

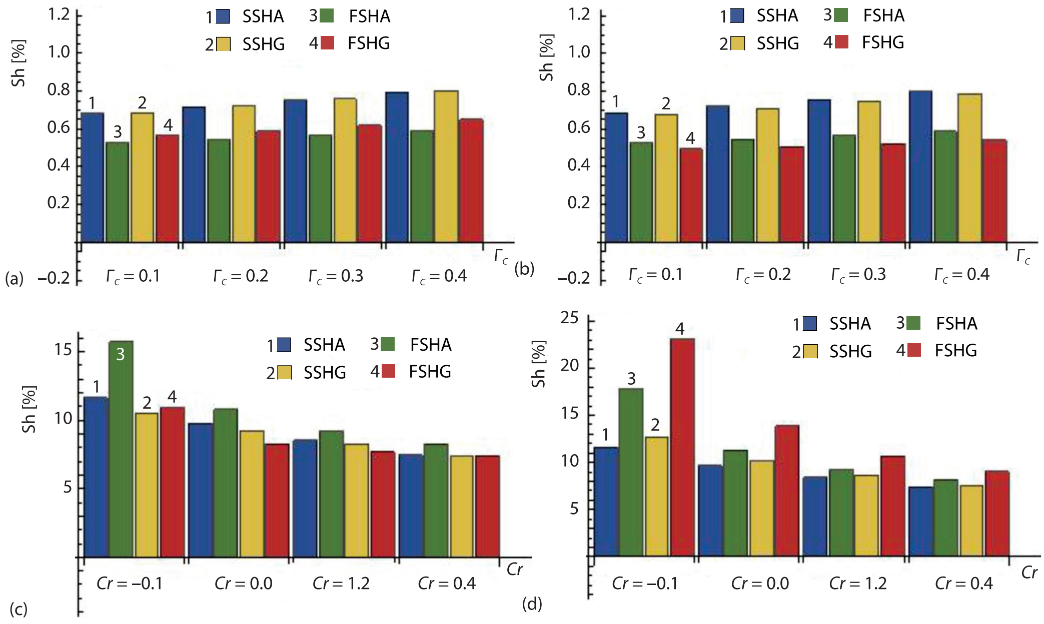

Figure 13. Variation percentage of local Sherwood number for various values of Γ_C (a) and (b) and Cr (c) and (d) with HA/HG for NH (a) and (c) and NC (b) and (d)

Conclusions

The purpose of this research paper is to investigate the outcomes of combined convective flow of a chemically reacting OBL with CCDF in the presence of second order slip, HA/HG and NH/NC. After our investigations, we found that he stream speed reduces with enhancing the velocity relaxation time parameter and it increases when raising the velocity retrardation time parameter. The thicker thermal boundary-layer is obtained in the presence of NH parameter and quite opposite trend is obtained in NC parameter. The decreasing rate of solutal boundary-layer thickness is high in generative chemical reaction case compared to the destructive chemical reaction case. The larger amount of heat transfer gradient is obtained in NH case compared to the NC case. The increasing rate of mass transfer is high in Fourier case compared to the non-Fourier case.

Nomenclature

A – positive constant
B_T – heat transfer spalding number
$\hat{C}$ – fluid concentration [kgm^{-3}]
C_f – skin friction coefficient
C_p – specific heat [Jkg^{-1}K^{-1}]
$\hat{C}_w$ – wall concentration
$\hat{C}_\infty$ – free stream concentration
$\hat{D}_B$ – mass diffusivity
$\hat{g}$ – acceleration due to gravity
F_w – suction/injection parameter
F' – non-dimensional velocity
Gr_x^* – concentration buoyancy number
Gr_x – thermal buoyancy number
Hg – heat generation/absorption parameter
k – thermal conductivity, [Wm^{-1}K^{-1}]
k^* – mean absorption coefficient
k_1 – chemical reaction rate
N_T – Newtonian heating parameter
Pr – Prandtl number
Q – heat generation/absorption coefficient
R – radiation parameter
Re_x – Reynolds number
Ri – Richardson number
Sc – Schmidt number
$\hat{T}$ – fluid temp
$\hat{T}_w$ – wall tempe
$\hat{u}$ and $\hat{v}$ – velocity components, [ms^{-1}]
$\hat{x}$ and $\hat{y}$ – direction co-ordinates, [m]

Greek symbols

$\hat{\alpha}$ – thermal diffusivity, [m^2s^{-1}]
α_1 – relaxation time constant
α_2 – retardation time constant
$\beta_{\hat{C}}$ – coefficient of concentration expansion, [$kg^{-1}m^3$]
$\beta_{\hat{T}}$ – coefficient of thermal expansion, [K^{-1}]
Γ_C – mass relaxation parameter
Γ_T – thermal relaxation parameter
η – dinensional variable
Θ – non-dimensional temperature
$\hat{\lambda}_1$ – relaxation time of heat flux
$\hat{\lambda}_2$ – relaxation time of mass flux
ν – kinematic viscosity, [m^2s^{-1}]
ρ – fluid density, [kgm^{-3}]
σ^* – Stefan Boltzmann constant, [$Wm^{-2}K^{-4}$]
Φ – non-dimensional concentration

Acknowledgment

This project was funded by the Deanship of Scientific Research (DSR), King Abdulaziz University, Jeddah, Saudi Arabia, under Grant No. D-257-130-1440. The authors, therefore, acknowledge with thanks DSR technical and financial support.

References

[1] Oldroyd, J. G., The Formulation of Rheological Equations of State, *Proceedings of the Royal Society of London Series*, *200* (1950), pp. 523-541
[2] Rajagopal, K. R., Bhatnagar, P. K., Exact Solutions for Some Simple Flows of an Oldroyd-B Fluid, *Acta Mechanica*, *113* (1995), Mar., pp. 233-239
[3] Farooq, A., *et al*., Soret and Dufour Effects on 3-D Oldroyd-B Fluid, *Physica A: Statistical Mechanics and its Applications*, *503* (2018), Aug., pp. 345-354
[4] Fetecau, C., *et al*., On the Energetic Balance for the Flow of an Oldroyd-B Fluid Due to a Flat Plate Subject to a Time-Dependent Shear Stress, *Computers and Mathematics with Applications*, *60* (2010), 1, pp. 74-82
[5] Liu, Y., *et al*., Unsteady Helical Flow of a Generalized Oldroyd-B Fluid with Fractional Derivative, *International Journal of Mathematics Trends and Technology*, *5* (2014), 1, pp. 66-76
[6] Jamil, M., *et al*., Unsteady Helical Flows of Oldroyd-B Fluids, *Communications in Non-Linear Science and Numerical Simulation*, *16* (2011), 3, pp. 1378-1386
[7] Motsa, S. S., Ansari, M. S., Unsteady Boundary-Layer Flow and Heat Transfer of Oldroyd-B Nanofluid Towards a Stretching Sheet with Variable Thermal Conductivity, *Thermal Science*, *19* (2015), Suppl. 1, pp. S239-S248
[8] Fourier, J. B. J., *Theorie Analytique De La Chaleur*, Chez Firmin Didot, Paris, France, 1822
[9] Cattaneo, C., Sulla conduzione del calore, *Atti. Semin. Mat. Fis Univ. Modena Reggio Emilia, 3* (1948), pp. 83-101
[10] Christov, C. I., On Frame Indifferent Formulation of the Maxwell-Cattaneo Model of Finite Speed Heat Conduction, *Mechanics Research Communications*, *36* (2009), 4, pp. 481-486
[11] Asmadi, M. S., *et al*., Finite Difference Solution of Convective Flow of Upper-Convected Maxwell Fluid over a Horizontal Wedge with Suction and Heat Generation Using Cattaneo-Christov Heat Flux Model, *Thermal Science*, *25* (2021), 2A, pp. 1013-1021
[12] Mustafa, M., An Analytical Treatment for MHD Mixed Convection Boundary-Layer Flow of Oldroyd-B Fluid Utilizing non-Fourier Heat Flux Model, *International Journal of Heat and Mass Transfer*, *113* (2013), Oct., pp. 1012-1020
[13] Sui, J., *et al*., Boundary-Layer Heat and Mass Transfer with CattaneoeChristov Double-Diffusion in Upper-Convected Maxwell Nanofluid Past a Stretching Sheet with Slip Velocity, *International Journal of Thermal Sciences*, *104* (2016), June, pp. 461-468
[14] Dogonchi, A. S., Ganji, D. D., Impact of Cattaneo-Christov Heat Flux on MHD Nanofluid-Flow and Heattransfer between Parallel Plates Considering Thermal Radiation Effect, *Journal of the Taiwan Institute of Chemical Engineers*, *80* (2017), Nov., pp. 52-63
[15] Mallawi, F. M., *et al.*, Impact of Double-Stratification on Convective Flow of a Non-Newtonian Liquid in a Riga Plate with Cattaneo-Christov Double-Flux and Thermal Radiation, *Ain Shams Engineering Journal*, *12* (2021), 1, pp. 969-981
[16] Khan, S. U., *et al.*, Heat Transfer Analysis Based on Cattaneo-Christov Heat Flux Model and Convectiveboundary Conditions for Flow over an Oscillatory Stretching Surface, *Thermal Science*, *23* (2019), 2A, pp. 443-455

[17] Mehmood, T., *et al*., Transverse Thermopherotic MHD Oldroyd-B Fluid with Newtonian Heating, *Results in Physics*, *8* (2018), Mar., pp. 686-693
[18] Ramzan, M., *et al.*, The 3-D Flow of an Oldroyd-B Fluid with Newtonian Heating, *International Journal of Numerical Methods for Heat and Fluid-Flow*, *25* (2015), 1, pp. 68-85
[19] Patil, P. M., *et al*., Unsteady Thermal Radiation Mixed Convection Flow from a Moving Vertical Plate in a Parallel Free Stream: Effect of Newtonian Heating, *International Journal of Heat and Mass Transfer*, *62* (2013), July, pp. 534-540
[20] Lesnic, D., *et al*., Free Convection Boundary-Layer Flow Along a Vertical Surface in a Porous Medium with Newtonian Heating, *International Journal of Heat and Mass Transfer*, *42* (1999), 4, pp. 2621-2627
[21] Zhu, T., *et al.*, Second-Order Slip MHD Flow and Heat Transfer of Nanofluids with Thermal Radiation and Chemical Reaction, *Applied Mathematics and Mechanics (English Edition)*, *36* (2015), 9, pp. 1131-1146
[22] Das, K., *et al*., Effect of Magnetic Field on Oldroyd-B Type Nanofluid-Flow over a Permeable Stretching Surface, *Propulsion and Power Research*, *7* (2018), 3, pp. 238-246
[23] Jagan, K., *et al.*, Soret and Dufour Effect on MHD Jeffrey Nanofluid-Flow Towards a Stretching Cylinder-with Triple Stratification, Radiation and Slip, *Defect and Diffusion Forum*, *387* (2018), Sept., pp. 523-533
[24] Kasmani, R. M., *et al*., Effect of Chemical Reaction on Convective Heat Transfer of Boundary-Layer Flow in Nanofluid over a Wedge with Heat Generation/Absorption and Suction, *Journal of Applied Fluid Mechanics*, *9* (2016), 1, pp. 379-388
[25] Niranjan, H., *et al.*, Chemical Reaction, Soret and Dufour Effects on MHD Mixed Convection Stagnation Point Flow with Radiation and Slip Condition, *Scientia Iranica, Transaction B, Mechanical Engineering, 24* (2017), 2, pp. 698-706
[26] Eswaramoorthi, S., *et al*., Soret and Dufour Effects on Viscoelastic Boundary-Layer Flow, Heat and Mass Transfer in a Stretching Surface with Convective Boundary Condition in the Presence of Radiation and Chemical Reaction, *Scientia Iranica, Transaction B, Mechanical Engineering*, 23 (2016), 6, pp. 2575-2586
[27] Sivasankaran, S., *et al*., Chemical Reaction, Radiation and Slip Effects on MHD Mixed Convection Stagnation-Point Flow in a Porous Medium with Convective Boundary Condition, *International Journal of Numerical Methods for Heat & Fluid-Flow*, *27* (2017), 2, pp. 454-470
[28] Bhuvaneswari, M., *et al*., Effect of Viscous Dissipation and Convective Heating on Convection Flow of a Second Grade Fluid over a Stretching Surface: Analytical and Numerical Study, *Scientia Iranica. Transaction B, Mechanical Engineering*, *26* (2019), 3, pp. 1350-1357
[29] Abel, M. S., *et al*., The MHD Flow and Heat Transfer for the Upper-Convected Maxwell Fluid over a Stretchingsheet, *Meccanica*, *47* (2012), July, pp. 385-393
[30] Waqas, M., *et al.*, Stratified Flow of an Oldroyd-B Nanoliquid with Heat Generation, *Results in Physics*, *7* (2017), June, pp. 2489-2496

Paper submitted: October 3, 2019
Paper revised: July 4, 2020
Paper accepted: July 12, 2020